Apolipoprotein E isoform-specific phase transitions in the retinal pigment epithelium drive disease phenotypes in age-related macular degeneration

Authors:

Nilsa La Cunza[1, 2], Li Xuan Tan[1], Gurugirijha Rathnasamy[5], Thushara Thamban[1], Colin J. Germer[1,2], Kimberly A. Toops[4] and Aparna Lakkaraju[1, 2, 3, *]

Affiliations:

[1]Department of Ophthalmology, School of Medicine, University of California, San Francisco, CA, USA

[2]Pharmaceutical Sciences and Pharmacogenomics Graduate Program, University of California, San Francisco, CA, USA

[3]Department of Anatomy, School of Medicine, University of California, San Francisco, CA, USA

Present address: [4]Zeiss Microscopy, New York; [5]TurtleTree Labs, Singapore

***Correspondence to:**

Aparna Lakkaraju (Aparna.Lakkaraju@ucsf.edu), Department of Ophthalmology, University of California, San Francisco, 10 Koret Way, Room 233, San Francisco, CA 94143.

Abstract

The retinal pigment epithelium (RPE) is the site of initial damage leading to photoreceptor degeneration and vision loss in age-related macular degeneration (AMD). Genetic and histopathological studies implicate cholesterol dysregulation in AMD; yet mechanisms linking cholesterol to RPE injury and drusen formation remain poorly understood. Especially enigmatic are allelic variants of the cholesterol transporter *APOE*, major risk modifiers in Alzheimer's disease that show reversed risk associations with AMD. Here, we investigated how ApoE isoforms modulate RPE health using live-cell imaging of primary RPE cultures and high-resolution imaging of human donor tissue. We show that the AMD-protective ApoE4 efficiently transports cholesterol and safeguards RPE homeostasis despite cellular stress. In contrast, ApoE2-expressing RPE accumulate cholesterol, which promotes autophagic deficits and complement-mediated mitochondrial fragmentation. Redox-related order-disorder phase transitions in ApoE2 drive the formation of intracellular biomolecular condensates as potential drusen precursors. Drugs that restore mitochondrial function limit condensate formation in ApoE2-RPE. Autophagic and mitochondrial defects correlate with intracellular ApoE aggregates in AMD donor RPE. Our study elucidates how AMD risk variants act as tipping points to divert the RPE from normal aging towards AMD by disrupting critical metabolic functions, and identifies mitochondrial stress-mediated aberrant phase transitions as a novel mechanism of drusen biogenesis.

Age-related macular degeneration (AMD), a complex neurodegenerative disease that destroys central high-resolution vision, is the most common cause of permanent blindness in older adults. Global AMD prevalence is projected to exceed 200 million by the year 2040 largely due to lack of treatments for non-neovascular AMD, which affects the majority of patients (1, 2). The primary site of injury in AMD is the retinal pigment epithelium (RPE), a monolayer of postmitotic polarized cells that performs numerous functions essential for photoreceptor health and for vision (3, 4). In early AMD, RPE dysfunction is accompanied by the deposition of extracellular aggregates called drusen, which are rich in cholesterol and apolipoprotein E (ApoE) (5-7). Clinically, RPE abnormalities and drusen location, size, and morphology are strong predictors of AMD progression (1). Polymorphisms in over 50 independent genes involved in regulating complement activation, cholesterol homeostasis, oxidative stress and extracellular matrix remodeling are associated with AMD. Yet, we have limited insight into the mechanisms by which disease-associated variants promote RPE injury, drusen biogenesis, and subsequent vision loss (7-9).

The RPE is a regulatory hub for cholesterol and lipid transport into and out of the retina, and several independent lines of investigation suggest that impaired RPE cholesterol metabolism promotes AMD pathogenesis (10). Genetic variants in the cholesterol transporters *APOE* and ATP-binding cassette transporter A1 *(ABCA1)* and the HDL remodeling proteins cholesterol ester transfer protein (*CETP*) and hepatic lipase (*LIPC*) are associated with AMD (8, 11). As these genes are all expressed by the RPE, it is plausible that the disease-associated variants act locally to modulate cholesterol transport and lipoprotein metabolism in the retina (10). Confirming a direct link between RPE cholesterol levels and retinal degeneration, RPE-specific deletion of *ABCA1* in mice leads to cholesterol storage in the RPE, followed by progressive RPE atrophy, photoreceptor loss and retinal degeneration (12). Mechanistically, we have shown that excess RPE cholesterol derails microtubule-based transport,

which impairs autophagy and makes the RPE susceptible to complement-induced mitochondrial injury in models of macular degeneration (13-15). These studies underscore the need for strictly regulating RPE cholesterol, because it impacts several homeostatic mechanisms, including metabolism and inflammation, whose dysfunction contributes to AMD (7).

Of the cholesterol genes implicated in AMD, the role of *APOE* is particularly enigmatic because of the reversed risk associations with Alzheimer's disease. Humans are the only known species where the *APOE* gene has three common genetic variants arising from two polymorphisms (rs7412 and rs429358), which lead to cysteine/arginine interchanges at positions 112 and 158: ApoE2 has two cysteines, ApoE3 has a cysteine and an arginine, and ApoE4 has two arginines. The single amino acid changes between ApoE2, E3 and E4 substantially alter protein structure and function, including oligomer formation, and binding to lipids and receptors (16-20). *APOE4* is one of the strongest genetic risk factors for Alzheimer's disease, whereas *APOE2* is protective (21, 22). In contrast, *APOE4* significantly reduces the risk of developing AMD, and the *APOE2* allele is associated with increased susceptibility (8, 11, 23, 24). In the retina, the RPE is a primary biosynthetic source of ApoE and cholesterol, which are principal components of drusen. Long-term *in vitro* cultures of RPE exhibit basal ApoE-containing deposits, and this is increased by AMD-associated stressors such as complement activation (6, 25-28). However, precisely how *APOE* variants influence RPE function and drusen formation, and how this impacts disease susceptibility and progression are critical, unresolved questions in AMD biology.

Here, we hypothesized that the RPE could be a primary locus of pathogenic ApoE functions, and sought to identify the mechanisms by which ApoE isoforms differentially impact RPE health. We used high-speed live-cell imaging of polarized adult primary RPE cultures and high-resolution

imaging of human donor tissue to investigate autophagy, mitochondrial integrity and ApoE dynamics with unprecedented spatial and temporal detail. Our data show that ApoE3 and ApoE4 efficiently transport cholesterol, and help maintain RPE health under conditions of cellular stress. In contrast, ApoE2-expressing RPE accumulate excess cholesterol, which inhibits autophagy and promotes mitochondrial fragmentation in response to complement attack. All ApoE isoforms have intrinsically disordered domains (29), which could enable aberrant phase separation of these proteins in the cytosol (30). Our live-cell imaging studies helped us identify a novel biophysical mechanism for drusen biogenesis: redox status-related order-disorder transitions in ApoE2 driven by dysfunctional mitochondria, which induce the formation of intracellular ApoE biomolecular condensates within the RPE as likely precursors to drusen. Drugs that restore RPE mitochondrial health limit condensate formation in ApoE2-expressing RPE. Our study provides valuable insight into how a key AMD risk variant mediates crosstalk between lipid and complement pathways to disrupt critical metabolic functions in the RPE, and identifies oxidative stress-mediated aberrant phase transitions as an exciting new mechanism that could contribute to drusen biogenesis.

Results

Polarized adult primary RPE model for investigating isoform-specific ApoE functions. To date, humans are the only species known to express multiple allelic variants of *APOE,* with *APOE3* being the most and *APOE2* the least prevalent (~79% global allele frequency for *APOE3* compared to ~7% for *APOE2* and 14% for *APOE4*) (31) (Figure S1A). Mice, pigs and non-human primates express a single form of ApoE that has arginines at positions 112 and 158; however, ApoE in these species functions like human ApoE3 because it lacks arginine at position 61, and therefore cannot participate in the domain interaction seen in human ApoE4 (20, 32). Mice with targeted replacement of human *APOE3* and *APOE4* have been widely used to study the role of *APOE4* in Alzheimer's disease.

However, *APOE2* targeted replacement mice have a major limitation because ~100% of these mice develop type III hyperlipoproteinemia, unlike humans, where only 10% of those with the *E2/E2* genotype develop the disease (33). As *APOE2* mice have increased plasma levels of chylomicrons and VLDL remnants, this will likely influence lipoprotein and cholesterol levels in the RPE and retina, and could lead to confounding results. Studies on the retina show that aged transgenic mice expressing either human *APOE2* or *APOE4* fed a high-fat diet developed RPE vacuolization, pigmentation defects and Bruch's membrane thickening, whereas aged *APOE3* mice exhibited only minor RPE changes (34). In another study, however, *APOE4* expression prevented, and *APOE2* promoted, pathological sub-retinal inflammation in *Cx3cr1*$^{-/-}$ mice (35). iPSC-derived models of neurons and astrocytes from human donors homozygous for *E3* or *E4* or after gene editing *E3* to *E4* have recently been developed to model Alzheimer's disease (36, 37). While these models recapitulate important disease phenotypes, ApoE4-expressing astrocytes derived from different iPSC lines show markedly different profiles of ApoE4 expression and secretion likely reflecting the considerable variability across iPSC lines and the cells derived from them with regards to differentiation potential, epigenetic status and maturation characteristics (38, 39).

To avoid these potentially confounding issues, we chose to employ our well-characterized polarized adult primary porcine RPE cultures (40) transfected with fluorescently-tagged human ApoE2, E3 or E4 to investigate the functions of ApoE isoforms in the RPE. We have extensively used this model for live-cell imaging and have shown that it recapitulates critical disease phenotypes observed in human donor RPE and in mouse models of Stargardt inherited macular degeneration including lipofuscin-induced cholesterol accumulation, and consequent autophagic defects and complement-mediated mitochondrial injury (13-15). Pertinently, porcine *APOE* has a promoter polymorphism that decreases endogenous ApoE expression (41). This polymorphism is widespread in many domestic pig breeds including those used for harvesting RPE in our studies. In support of

this, we observed very low endogenous ApoE (~34 kDa) expression in our porcine RPE cultures (Fig. 1A), indicating that interference from endogenous ApoE would not be a significant factor in our studies.

To enable live imaging of ApoE isoforms, we transfected porcine primary RPE with plasmids encoding human ApoE2, E3 or E4 (42) tagged with either EGFP or mCherry at the C-terminus, which does not interfere with intracellular trafficking or secretion of ApoE (43-45). We observed comparable transfection efficiencies and expression of human ApoE fusion proteins (~61 kDa) (Figure 1A). As analyses of our live imaging data require quantification at the single-cell level, we measured mCherry fluorescence intensities (mean, maximum and sum) per cell and found no significant differences among the three isoforms (Figures S1B-D) suggesting that the three isoforms are expressed at equivalent levels in primary porcine RPE. These results validate the strengths of human ApoE-expressing primary porcine RPE cultures as an appropriate model to study isoform-specific functions of ApoE in the RPE.

Isoform-specific dynamic ApoE trafficking alleviates pathological cholesterol accumulation in the RPE. In the retina, cholesterol is required for maintaining photoreceptor disc membrane fluidity and rhodopsin activation (46, 47), and for membrane repair after injury (22). Bidirectional secretion of ApoE and other lipoproteins by polarized RPE likely plays an important role in shuttling cholesterol into and out of the retina (10). To identify isoform-specific differences in ApoE trafficking, and hence, cholesterol transport in the RPE, we performed high-speed live-cell imaging of primary polarized RPE cultures expressing mCherry-tagged human ApoE2, E3 or E4. Four-dimensional analysis of ApoE vesicle trajectories showed that a significantly greater population of ApoE3 and ApoE4 vesicles exhibited long-range, directed movements (large displacements) compared to ApoE2 (Figures 1B and 1C). There are at least two structural features that can explain these differences in trafficking amongst

ApoE isoforms (Figure S1A). First, intermolecular disulfide bonds between cysteines at positions 112 and 158 in ApoE2 lead to the formation of multimers that are retained within the cell, as reported for macrophages and adipocytes (48, 49). Second, ApoE4 adopts a closed conformation due to domain interactions via salt bridges between the N-terminal receptor binding domain and the C-terminal lipid-binding domain, whereas ApoE2 adopts the most open conformation and ApoE3 an intermediate conformation (50). Thus, compared to ApoE2, ApoE3 and ApoE4 have more compact, dynamic structures, which would enable efficient intracellular trafficking.

Because ApoE transports free and esterified cholesterol, triglycerides and fatty acids, we assessed free cholesterol and neutral lipid pools in RPE expressing ApoE2, E3 or E4 using filipin to label cholesterol (15) and Bodipy 493/503 to label lipid droplets (cholesteryl esters and triglycerides) (51). Consistent with their trafficking dynamics, ApoE2-RPE had more free cholesterol (Figure S1E) and lipid droplets (Figures 1D and 1E), whereas RPE expressing ApoE3 or ApoE4 had significantly less. The improved cholesterol transport by ApoE3 and ApoE4 agree with studies on astrocytes showing that compared with ApoE2, these isoforms associate better with lipids and cholesterol (50).

We and others have reported that the age-related and pathological accumulation of lipofuscin bisretinoids (composed of A2E and other vitamin A metabolites) in macular degenerations leads to a secondary accumulation of cholesterol in the RPE (13-15, 52). We therefore asked if the increased mobility of ApoE3 and ApoE4 vesicles mitigates the cholesterol storage seen in RPE with A2E. Biochemical measurements of total cell cholesterol showed that RPE expressing either ApoE3 or ApoE4 were resistant to A2E-induced cholesterol accumulation. However, RPE with ApoE2 had significantly more total cholesterol (Figure 1F), as a likely consequence of the decreased ApoE2-mediated lipid transport.

Taken together, these studies indicate that ApoE isoforms exhibit profound differences in intracellular trafficking and cholesterol transport, likely due to isoform-specific intermolecular

interactions (48-50, 53). Pertinently, these data suggest that dynamic long-range trafficking of ApoE3 and ApoE4 is essential for maintaining cholesterol homeostasis and circumventing lipofuscin-mediated cholesterol accumulation in the RPE.

ApoE2 aggravates autophagic defects induced by lipofuscin bisretinoids. In eukaryotic cells, cellular cholesterol controls multiple steps of organelle biogenesis and trafficking by regulating membrane dynamics and association with microtubules (54). We have shown that cholesterol-mediated activation of acid sphingomyelinase (ASMase) in the RPE increases ceramide levels, which prevents microtubule deacetylation. The resulting accumulation of stable, acetylated microtubules interferes with multiple steps of autophagy, including autophagosome biogenesis and trafficking (15). Building on these studies, we hypothesized that isoform-specific differences in ApoE-mediated cholesterol transport would impact microtubule dynamics and autophagy in RPE with A2E. To test this, we performed high-speed live-cell imaging of EGFP-LC3-labeled autophagosomes in ApoE2, E3 or E4-expressing primary RPE (Figures 2A and S2A; Supplementary Movies S1-S8). As we have previously reported (15), mock-transfected RPE with A2E had significantly fewer autophagosomes compared to control RPE cultures without A2E. Expression of ApoE3 or ApoE4, but not ApoE2, increased autophagosome numbers in RPE with A2E comparable to control levels (Figure 2B). Analysis of LC3 trafficking showed that autophagosomes in RPE with A2E had predominantly shorter tracks, with significantly lower mean speeds and displacements (Mock-transfected control vs mock-A2E, Figures 2C-E; Supplementary Movies S1 and S2). Expression of ApoE3 or ApoE4 corrected the A2E-induced disruption of long-range, directed movements of autophagosomes in RPE with A2E and restored autophagosome mean speeds, whereas ApoE2 expression was ineffective (Figures 2C-D and S2B-G; Supplementary Movies S3-S8).

We observed subtle autophagosome trafficking defects in ApoE2-RPE even without A2E (Figures S2D and S2F). As ApoE2-RPE accumulate more cholesterol (Figures 1E and S1E), which increases tubulin acetylation via ASMase activation, we stained ApoE2-, E3 and E4-RPE for acetylated tubulin. ApoE2-RPE had more acetylated microtubules compared to mock-transfected RPE, and this was further increased by A2E (Figures S2H and S2I). In agreement with the LC3 trafficking data, expression of ApoE3 or ApoE4 decreased acetylated tubulin in RPE with A2E.

Autophagy is an essential clearance mechanism for the post-mitotic RPE, where debris cannot be diluted by cell division (4). RPE from AMD donors exhibit several autophagic defects including decreased LC3B lipidation (a marker for autophagosome biogenesis) and accumulation of p62/SQSTM1 (a measure of completion of autophagy) (55, 56). The data presented above underscore the importance of RPE cholesterol as a regulator of critical metabolic functions like autophagy in the RPE, and suggest that normalizing cellular cholesterol to help preserve efficient autophagy in the aging and diseased RPE could be a mechanism by which AMD-protective genetic variants exert their beneficial effect.

ApoE2 exacerbates complement-mediated mitochondrial injury in the RPE. We have reported that in models of macular degeneration, increased tubulin acetylation in RPE with excess cholesterol renders them susceptible to complement attack by inhibiting innate protective mechanisms that depend on microtubule-based trafficking (14). These mechanisms include rapid recycling of CD59, a complement regulatory protein that prevents the assembly of the C5b-9 terminal membrane attack complex (MAC) pore on the cell membrane, and elimination of MAC pores by lysosome exocytosis. Interfering with these mechanisms allows MAC pores to persist on the RPE cell membrane, and the resulting increase in intracellular calcium eventually leads to mitochondrial fragmentation and oxidative stress (14).

Given this direct link between RPE cholesterol and complement activation, we investigated how ApoE isoforms influence the ability of the RPE to withstand complement attack. We captured RPE mitochondrial dynamics by live-cell imaging before and after exposure to normal human serum (NHS) as a source of complement (14). Reconstruction of mitochondrial volumes showed highly integrated mitochondria in mock-transfected and ApoE3- or E4-expressing RPE, in agreement with our previous finding that healthy RPE are resistant to complement attack. In contrast, mitochondria in ApoE2-expressing RPE were fragmented in response to NHS (Figures 3A and 3B), indicating that complement-regulatory mechanisms are disabled in ApoE2-RPE, likely due to increased tubulin acetylation. As expected, and in agreement with our published data, A2E rendered mock-transfected RPE vulnerable to NHS. In contrast to ApoE2-RPE, expression of ApoE3 or ApoE4 suppressed mitochondrial fragmentation in RPE with A2E after NHS exposure (Figures 3C and 3D), as a consequence of better cholesterol homeostasis, which preserves microtubule-based trafficking and hence efficient mechanisms to combat complement activation.

If complement-mediated mitochondrial fragmentation is due to excess RPE cholesterol and ASMase-mediated tubulin acetylation, then drugs that decrease cell cholesterol or inhibit ASMase (14, 15) should maintain RPE mitochondrial integrity after complement attack. In support of this hypothesis, inhibiting cholesterol biosynthesis with the lipophilic statin simvastatin, increasing cholesterol efflux with the liver X receptor (LXR) agonist T0901317, or inhibiting ASMase with desipramine all decreased complement-induced mitochondrial damage in both mock-transfected (Figures S3A and S3B) and ApoE2-expressing RPE with A2E after exposure to NHS (Figures 3E and 3F).

These data provide further evidence for multilayered crosstalk between cholesterol and complement pathways in maintaining or endangering RPE metabolic health, and yet again, demonstrate that genetic variants or pharmacological approaches that limit excess cholesterol

safeguard RPE mitochondrial integrity. In support of this, epidemiological and genetic studies show that high HDL cholesterol is associated with increased complement activation in AMD patients (57), and abnormal complement activation is accompanied by mitochondrial dysfunction in AMD donor RPE (58).

ApoE2 undergoes aberrant phase transitions to form biomolecular condensates in the RPE. Declining mitochondrial function has recently been implicated in driving abnormal phase transitions in proteins, leading to the formation of biomolecular condensates or aggregates within the cell (30). We were intrigued by this because complement exposure has been shown to increase the deposition of ApoE-containing aggregates by RPE cells in culture (26-28), but the underlying mechanisms remain unexplored. Based on our data, we hypothesized that mitochondrial dysfunction in response to complement attack would cause ApoE to undergo liquid-liquid phase separation, a recently discovered biophysical phenomenon that underlies the formation of cytoplasmic biomolecular condensates (59-62). Proteins that undergo phase separation are characterized by intrinsically disordered regions (IDRs) that enable them to engage in low-affinity interactions with one another (63). Studies on neurodegenerative diseases like amyotrophic lateral sclerosis (ALS) suggest that IDRs in pathogenic mutant proteins can induce structural changes in biomolecular condensates, leading to the formation of insoluble aggregates (64). As ApoE isoforms have IDRs (Figure S4A-C) (29), we hypothesized that aberrant phase transitions could drive ApoE condensate formation in the RPE as precursors to drusen. Moreover, because we observed ApoE isoform-specific effects on complement-mediated mitochondrial injury, we investigated whether this would translate to differences in condensate formation by ApoE2, E3 and E4.

Phase-separated liquid-like condensates (i) are roughly spherical shape; (ii) fuse with one another to minimize surface tension; and (iii) dynamically respond to changes in the subcellular

environment (63-67). Live-cell imaging showed that ApoE forms spherical structures with average sphericity ~0.9 (Figures 4A and 4B) that readily fuse and relax (Figure 4C), suggesting that ApoE2, E3 and E4 all segregate into liquid-like assemblies within the RPE. Although the three isoforms had similar disorder tendencies when analyzed by Meta-predictors such as DisMeta (66) and other commonly used disorder predictors (Figures S4A-C), there were significantly more ApoE2 condensates with larger volumes (> 0.6 μm^3), compared to either ApoE3 or ApoE4 condensates (Figures 4D and S4D-F). To establish the mechanism of formation of ApoE2 condensates, we tested two hypotheses. First, we treated ApoE2-expressing RPE for two minutes with 1,6-hexanediol, an aliphatic alcohol known to disrupt weak hydrophobic interactions that anchor biomolecular condensates (63, 65, 66). Consistent with our hypothesis of ApoE2 phase separation, we observed that 1,6-hexanediol treatment rapidly decreased both the number and volume of ApoE2 condensates in the RPE (Figures 4E and S4G).

Because biomolecular condensate formation is known to be exquisitely sensitive to intracellular environment (30), we next asked whether declining metabolic activity in ApoE2-RPE due to loss of mitochondrial function could increase the propensity for aberrant phase transitions. We analyzed condensate volumes in ApoE2-, ApoE3- and ApoE4-expressing RPE under conditions known to cause cellular stress and mitochondrial damage (i.e., exposure of RPE with A2E to complement). Our data show that whereas A2E alone did not noticeably impact condensate numbers or volumes, exposure of ApoE2-RPE with A2E to NHS significantly increased the number of large (> 0.6 μm^3) condensates (Figure 4F), consistent with our mitochondrial fragmentation data (Figures 3A-3D). We also observed a small but significant increase in large condensates in ApoE3-RPE exposed to A2E and NHS, whereas ApoE4-RPE were completely resistant to these stress-induced phase transitions (Figure 4F). To better understand the relationship between ApoE condensates and mitochondrial function, we used IUPRED2A (68) to predict redox-state dependent transitions in

ApoE isoforms. This modeling showed that ApoE2 undergoes more order-disorder phase transitions under oxidative stress compared to ApoE3 or ApoE4 (Figures S4H-J). ApoE2 has cysteine residues at positions 112 and 158, which can undergo reversible thiol oxidation in response to the intracellular redox environment. Pertinently, these thiol modifications enable ApoE2 to form disulfide-linked homodimers and higher-order oligomers (69-71), which would explain the increase in ApoE2 condensate volumes. In agreement with this model, ApoE3, which has a cysteine at 112 and an arginine at 158, is predicted to have fewer phase transitions under oxidative stress; however, thiol modification at 112 could presumably explain the small increase in condensate formation we observed in Figure 4F. In contrast, ApoE4 has arginines at both 112 and 158, and is therefore impervious to redox-state dependent phase transitions and oligomer formation (Figure S4J).

Finally, to confirm the role of mitochondria in driving ApoE2 phase transitions, we asked if drugs that prevent mitochondrial injury after complement attack limit condensate formation. Treatment with either desipramine, simvastatin or T0901317 significantly decreased the fraction of large ApoE2 condensates in RPE with A2E exposed to complement (Figure 4G). Collectively, these findings demonstrate that aberrant phase separation is a novel mechanism that could nucleate intracellular ApoE2 condensates within the RPE, especially under conditions of declining mitochondrial health. Further, pharmacological approaches that safeguard RPE metabolic function could limit the formation of ApoE2 condensates.

Autophagic and mitochondrial defects correlate with intracellular ApoE aggregates in AMD donor RPE. To date, studies on ApoE have almost exclusively focused on its presence in sub-RPE and sub-retinal drusen in AMD donors (5, 6, 72), and we have little information regarding ApoE aggregates *within* the RPE and how these intracellular condensates might correlate with disease. To address this and to extend our live imaging data to human donors, we asked if the number and volume of ApoE

aggregates within the RPE reflected the extent of RPE metabolic dysfunction, and if this in turn correlated with AMD.

We immunostained macular retinal cryosections from unaffected donors and donors with non-neovascular AMD with validated antibodies to the autophagy substrate p62/SQSTM1, the mitochondrial membrane protein TOM20 and ApoE. High-resolution imaging of RPE with discernible and contiguous plasma membrane as defined by phalloidin staining showed significantly more p62 puncta within AMD donor RPE compared to unaffected controls, indicating a block in autophagic flux (Figures 5A, 5B and S5). Volume reconstructions and analysis of TOM20-stained mitochondria showed that mitochondrial networks were highly fragmented in AMD RPE compared to unaffected donors (Figures 5C, 5D and S5). Analysis of intracellular ApoE staining in intact RPE showed that the number and volume of ApoE aggregates correlated positively with the extent of autophagic and mitochondrial defects in the RPE and with AMD (Figures 5E, 5F and S5).

There were a few significant caveats to these experiments: first, although we genotyped donors for AMD-associated risk alleles (*CFH, C3, HTRA1/ARMS2*, *APOE, ABCA1* and *CETP*), our small sample size precluded any clear genotype-phenotype correlations (Tables S2 and S3). Second, because of the extremely low frequency of E2 and E4 alleles in the general population (~0.4-2% prevalence of *E2/E2*, *E2/E4* or *E4/E4* genotypes; ~10% for *E2/E3*) (31)) we were unable to obtain tissue from donors with these genotypes. Third, the limited availability of AMD donor tissue with intact RPE required for high-resolution imaging that could be obtained within a reasonable death-to-preservation time (~10 h) further decreased our sample size.

Although our small sample size with four donors and two *APOE* genotypes prevents us from drawing major conclusions, we observed that Donor 1 (unaffected) and donor 3 (with AMD) both had AMD-associated SNPs in *CFH, C3* and *ABCA1*, but differed in their *APOE* genotype (*E3/E4 vs E3/E3*). Donor 1, with one *E4* allele, had better RPE metabolic health and fewer ApoE aggregates,

which would support our model of redox-dependent phase transitions in ApoE3 due to the cysteine at position 112. Donor 2 (unaffected) and donor 4 (with AMD) both had the *E3/E3* genotype but differed in almost all other major AMD risk alleles (Table S1). A major difference was that the unaffected donor had the non-risk *CFH* allele, whereas the AMD donor had the *Y402H* allele, which has been associated with increased mitochondrial DNA damage (58). The complex genetics and multifactorial etiology of AMD make it challenging to ascribe individual genetic polymorphisms to specific disease phenotypes (8). However, these data show that AMD donor RPE exhibit the trifecta of disrupted autophagy, mitochondrial fragmentation and intracellular ApoE aggregates. Although analysis of fixed tissue provides only a snapshot in time, taken together with the live imaging data, our studies suggest that conditions that lead to metabolic stress – whether it occurs via cholesterol accumulation, complement activation or other pathways – could trigger ApoE phase separation within the RPE, which could over time nucleate drusen.

Discussion

ApoE is a pleiotropic protein with critical roles in cholesterol transport, metabolism, immunity and inflammation (73, 74). *APOE* variants have emerged as major risk modifiers for a growing number of diseases, with *APOE4* conferring increased risk in some (e.g., Alzheimer's disease, coronary artery disease, vascular dementia) and protection in others (e.g., AMD, primary tauopathy, melanoma, type 2 diabetes) (8, 22, 75, 76). How ApoE isoforms influence disease pathogenesis in many of these conditions, however, remains unclear. Here, we investigated the impact of ApoE isoforms on RPE health and function because the RPE is the central regulator of cholesterol homeostasis in the retina, the primary biosynthetic source of ApoE, and a key site of injury in AMD (6, 10, 77). Using advanced live-cell imaging of polarized adult primary RPE cultures and high-resolution imaging of human donor tissue, our studies identify novel mechanisms by which ApoE2 predisposes the RPE towards,

and ApoE4 safeguards the RPE from, AMD-associated phenotypes. These studies provide a cellular framework to interpret genetic and epidemiological data on the role of ApoE isoforms in RPE injury and in AMD.

Our data suggest that cholesterol homeostasis in the RPE is the fulcrum that regulates major biological pathways implicated in AMD including autophagy, complement regulation, mitochondrial integrity and drusen biogenesis (7). The dynamic trafficking and efficient cholesterol transport mediated by ApoE3 and ApoE4 correlate with their ability to maintain RPE metabolic health in the presence of innate stressors associated with aging and AMD such as lipofuscin and complement activation (78). In contrast, the constrained trafficking of ApoE2 promoted cholesterol accumulation in ApoE2-RPE, leading to compromised autophagy and increased vulnerability of the RPE to complement attack. Accumulation of lipid droplets, autophagic defects and mitochondrial abnormalities have been observed in AMD donor RPE (55, 56, 58, 79), and our studies provide a molecular mechanism to explain how AMD-associated cholesterol pathway genes can drive these phenotypes.

A significant and exciting advance from our live imaging studies is the discovery of aberrant ApoE phase transitions as a potential early trigger for drusen biogenesis. Proteomics of drusen components (80), and deposition of sub-RPE ApoE aggregates by long-term (~3-6 months) cultures of polarized human and porcine RPE (25-28, 81) suggest that drusen originate from the RPE (82). However, these observational studies do not address a critical question in AMD biology: how does ApoE nucleate drusen within the RPE, and can we target this therapeutically? We now show that mitochondrial stress stimulates redox state-mediated aberrant phase transitions in ApoE2 because of cysteines at positions 112 and 158, whereas ApoE4 is resistant to these phase transitions. In this regard, it is worth noting that ApoE3-expressing RPE also exhibit increased phase transitions and aggregates, albeit to a lesser

extent than ApoE2-RPE, because of the single cysteine at 112. Given the low prevalence of *APOE2* and *APOE4* alleles, these data support the multiple-hit model of AMD pathogenesis where the increased propensity of ApoE3 phase transitions could be either exacerbated by additional genetic risk alleles such as *CFH*, for instance, or environmental factors like smoking (7, 8, 79). Indeed, our high-resolution imaging of AMD donor RPE where the extent of RPE metabolic stress (decreased autophagy and increased mitochondrial fragmentation) correlated with the number and volume of ApoE aggregates in *E3/E3* donors lends strong support to this model.

There could be at least two mechanisms by which intracellular ApoE phase transitions lead to sub-retinal or sub-RPE drusen deposition. First, ApoE aggregates could undergo directed exocytosis similar to that reported in macrophages in contact with immune complexes (83). In support of this, acetylated microtubules aid the exocytosis of secretory granules in mast cells (84). Second, binding of ApoE to ABCA1 on the plasma membrane modulates both ApoE lipidation and cholesterol efflux. A recent study comparing ApoE3 with E4 showed that ApoE4 had a greater ABCA1 binding affinity in CNS astrocytes (ApoE2 was not studied) (85). Genetic variants in ABCA1 are also implicated in AMD (8), and mouse models with RPE-specific deletion of ABCA1 show RPE atrophy and retinal degeneration (12). While the relative contributions of these mechanisms in the exocytosis of ApoE condensates remains to be investigated, it is tempting to speculate that AMD-risk alleles of *APOE* and *ABCA1* could synergize to drive drusen deposition.

Our data show that drugs that increase cholesterol efflux or inhibit ASMase maintain RPE metabolic health and prevent aberrant phase separation in ApoE2-expressing RPE. Several retrospective studies have analyzed the relationship between statin use and AMD, with inconclusive results (86). A small open label prospective study of prolonged treatment with high-dose statins reported drusen regression

in a subset of patients (87). However, these studies were not stratified according to *APOE* genotype, which is known to modify the response to statins (88). Several FDA-approved drugs are known to inhibit ASMase as an off-target effect, including the anti-depressant desipramine that was used in this study. Retrospective studies using pooled epidemiological data from three continents show that desipramine use is associated with a significant decrease in susceptibility and progression of early AMD (89). These studies suggest that further investigation of cholesterol-lowering drugs and ASMase inhibitors in AMD, stratified by risk genotype, is warranted.

Recent studies have identified several intriguing functions for ApoE beyond its well-described role in cholesterol transport. These include binding to complement proteins such as C1q and CFH (90, 91) in immune cells, modulating tau phosphorylation (75), phagocytosis and synaptic pruning (92), regulating glycolysis and metabolic coupling (93-95) in the brain, and pigmentation in melanocytes (96). Many of these functions have obvious relevance for the health and function of the retina and the RPE. Whether and how ApoE isoforms regulate these functions in the RPE and the retina are intriguing questions that should provide fertile ground for future investigations in retinal biology and AMD pathogenesis.

Developing effective therapies for AMD is predicated on understanding the biology behind genetic underpinnings of this complex disease. This is especially important for major risk variants like *APOE*, whose isoform-specific functions in the RPE and in AMD have been difficult to pin down (97). By establishing how ApoE isoforms modulate major AMD-associated biological pathways to drive RPE dysfunction and drusen nucleation, our study provides valuable insight into the role of AMD risk variants as “tipping points” that divert the RPE from normal aging towards AMD, and suggests that

therapeutically targeting regulatory mechanisms that maintain cholesterol homeostasis could be beneficial in limiting RPE injury and drusen formation in AMD.

Experimental Methods

(Detailed information about reagents, sources, and experimental methods are provided in the Supplementary Information. Brief methods are given below.)

Primary porcine RPE culture. RPE were isolated from freshly harvested porcine retinas using established protocols (40)**.** For live imaging, primary RPE were plated at confluence (~ 300,000 cells/cm^2) on serum-coated glass-bottom dishes (Mattek) as described (15, 40).

Expression of EGFP or mCherry-tagged ApoE isoforms in primary RPE. pcDNA3.1 plasmids expressing human ApoE2, E3 and E4 were provided by Dr. Joachim Herz (University of Texas Southwestern Medical Center, Dallas, TX) (42). EGFP or mCherry-tagged constructs were generated by inserting the ApoE2, E3 or E4 cDNA into the p-EGFP-N1 or p-mCherry-N1 vector (Invitrogen) between the XhoI and BamHI restriction sites. Sequences of the constructs was confirmed by UW-Madison Biotechnology Core and by Quintara (South San Francisco, CA). Primary porcine RPE were transfected with EGFP or mCherry-tagged ApoE2, E3 or E4 (Amaxa Nucleofector II, Lonza, Rockland, ME). Approximately 1.5 million cells and 5 μg plasmid DNA were used for each transfection. Cells were plated at confluence (300,000 cells/sq.cm) in growth medium on serum-coated glass-bottom dishes (MatTek, Ashland, MA) and used for live imaging 48-72 h later. Transfection efficiencies were ~30-40% for each of the isoforms.

Treatments and assays. Primary RPE cultures were treated with A2E (10 μM for 6 h and 48 h chase) to match levels found in aging human RPE (15, 98). Other reagents used the ASMase inhibitor desipramine (10 μM, 3 h, Sigma), the LXRα agonist T0901317 (1 μM for 16 h, Cayman Chemicals) and the lipophilic statin Simvastatin (5 μM for 16 h, Cayman Chemicals) (15, 99). Cholesterol levels were measured from RPE lysates using the Amplex Red cholesterol assay kit (ThermoFisher) (15).

Live imaging and analysis of ApoE trafficking. mCherry-ApoE2, E3 or E4 expressing primary porcine RPE cell cultures were imaged using the Andor Revolution XD with 100X/1.49 NA Apo TIRF objective (Nikon, Melville, NY) for ∼50 frames at 37°C. Trafficking data were collected from three separate transfections for a total of at least 17–23 movies captured per condition with the same laser power, exposure and electron-multiplying gain settings for all conditions. For analysis of trafficking parameters, ApoE-labeled vesicles were subjected to surface reconstruction using the Surfaces and Tracks modules and track length, track displacement and track lifetimes were calculated using Imaris v 8.7.4 (Bitplane, Concord, MA).

Immunoblotting. RPE lysates were resolved in 4-12% NuPAGE® Bis-Tris Precast gels (Invitrogen) and probed with antibodies to ApoE (1:300; Dako) and beta-tubulin (1:1000; Sigma) followed by horseradish peroxidase-conjugated secondary antibodies and visualized by ECL (Thermo Fisher). Bands were quantified using Image Studio (LI-COR, Lincoln, NE) and ApoE levels were normalized to that of beta-tubulin.

Neutral lipid and cholesterol staining. To analyze neutral lipids, mCherry-ApoE2, E3 or E4 expressing primary porcine RPE cell cultures were treated with Bodipy-493/503 (10 μM for 30 min at 37ºC, ThermoFisher), fixed in 2% paraformaldehyde and imaged. The number of Bodipy493/503

positive vesicles were quantified by the Spots module (Imaris). To analyze free cholesterol, cells were fixed and stained with 50 μg/ml filipin for 45 min (Sigma-Aldrich, St. Louis, MO) and imaged immediately. Intracellular filipin fluorescence was quantified by using Imaris.

Live imaging and analysis of autophagosome biogenesis and trafficking. mCherry-ApoE2, E3 or E4 expressing primary porcine RPE cell cultures were transduced with LC3B-GFP (ThermoFisher, Waltham, MA) for 16-24 hours. Autophagosome trafficking was monitored by live imaging and analysis of autophagosome numbers and trafficking parameters was performed using Imaris as previously described (15).

Live imaging of mitochondrial dynamics. mCherry-ApoE2, E3 or E4 expressing primary porcine RPE cell cultures ± A2E (10 μM for 6 h followed by a 48-h chase in fresh culture medium) were exposed to 10% NHS for 10 min (14). Cells were incubated with 0.2 μM MitoTracker Deep Red (ThermoFisher, Waltham, MA) for 15 min at 37ºC and imaged immediately. For analysis of mitochondrial volume, MitoTracker-labeled mitochondria were subjected to surface reconstruction in Imaris and automated segmentation by color-coding based on volume of the connected components was used for 3D surface rendering of mitochondria.

Analysis of ApoE condensate dynamics. mCherry-ApoE2, E3 or E4 expressing primary porcine RPE cell cultures were imaged live using the same imaging conditions and parameters established for imaging ApoE trafficking to capture volume, fusion and fission events. In some experiments, mCherry-ApoE2-expressing RPE were treated with 0.5% 1,6 hexanediol (Sigma Aldrich, St. Louis, MO) in digitonin or digitonin alone (vehicle) to disrupt weak hydrophobic interactions or with T0901317, Simvastatin or desipramine as above. Condensate volumes were quantified by 3D surface

reconstruction and measuring mCherry fluorescence intensity per pixel of each condensate per z-plane of the confocal image. Histograms of number and volumes of ApoE condensates was constructed using Matlab (MathWorks, Natick, MA).

Genotyping and immunostaining of human donor globes. Globes from unaffected human donors and donors diagnosed with AMD were obtained from Lions Gift of Sight (Saint Paul, MN) with de-identified demographics (Table S2) and fundus photographs. DNA was extracted from frozen donor retinal tissue (PureLink Genomic DNA Kit, ThermoFisher, Waltham, MA), amplified by PCR using specific primers before genotyping (Quintara) ((8, 58, 100) Table S3). Cryosections of donor retina were stained with antibodies to p62/SQSTM1 (Novus NBP148320, 1:200), TOM20 (Santa Cruz sc-11415, 1:200) and ApoE (Genetex GTX100053 1:200). Sections were labeled with Alexa-Fluor conjugated secondary antibodies, Rhodamine-phalloidin and DAPI to label to label the actin cytoskeleton and nuclei, respectively. Sections were imaged by spinning disc confocal microscopy and analyses of p62 puncta, mitochondrial fragments and volume of ApoE structures were performed as described above.

Statistics. Data were analyzed using either one-way ANOVA with Bonferroni post- test or multiple *t*-test with Welch's correction for unequal variances (GraphPad Prism). Unless otherwise stated, data are presented as mean ± SEM of ≥3 independent experiments, with ≥ three replicates per condition per experiment.

Supplementary information

Supplementary Information includes detailed Experimental Methods, five figures, eight movies and three tables.

Acknowledgements

We thank Joachim Herz for the human *APOE2*, *APOE3* and *APOE4* constructs and Jimmy Pham for help with Matlab analyses. This research was supported by NIH/NEI grants R01EY023299 and R01EY030668, the Research to Prevent Blindness Catalyst Award for Innovative Approaches to AMD, the BrightFocus Foundation Award for AMD research M2015350, Macular Society UK, and the Retina Research Foundation Rebecca Meyer Brown Professorship (AL), NIH/NEI Diversity Supplement Fellowship (NLC) and NIH/NEI P30 core grants to the University of Wisconsin-Madison (EY016665) and to the University of California, San Francisco (EY002162).

Author Contributions:

NLC, LXT, KAT and AL designed the study; NLC, LXT and KAT performed the experiments; KAT, LXT, GR and CJG generated primary RPE cultures; NLC, GR and CJG processed human donor tissues; TT and NLC performed the genotyping; NLC, LXT, KAT and AL analyzed the data; GR and TT critically reviewed the manuscript; NLC, KAT, LX, CJG and AL wrote the manuscript.

References

1. Wong WL, Su X, Li X, Cheung CM, Klein R, Cheng CY, et al. Global prevalence of age-related macular degeneration and disease burden projection for 2020 and 2040: a systematic review and meta-analysis. *The Lancet Global health.* 2014;2(2):e106-16.
2. Dolgin E. Age-related macular degeneration foils drugmakers. *Nat Biotechnol.* 2017;35(11):1000-1.

3. Caceres PS, and Rodriguez-Boulan E. Retinal pigment epithelium polarity in health and blinding diseases. *Curr Opin Cell Biol.* 2020;62:37-45.

4. Lakkaraju A, Umapathy A, Tan LX, Daniele L, Philp NJ, Boesze-Battaglia K, et al. The cell biology of the retinal pigment epithelium. *Prog Retin Eye Res.* 2020:100846.

5. Malek G, Li C-M, Guidry C, Medeiros NE, and Curcio CA. Apolipoprotein B in cholesterol-containing drusen and basal deposits of human eyes with age-related maculopathy. *Am J Pathol.* 2003;162:413-25.

6. Anderson DH, Ozaki S, Nealon M, Neitz J, Mullins RF, Hageman GS, et al. Local cellular sources of apolipoprotein E in the human retina and retinal pigmented epithelium: Implications for the process of drusen formation. *Am J Ophthalmol.* 2001;131:767-81.

7. Handa JT, Bowes Rickman C, Dick AD, Gorin MB, Miller JW, Toth CA, et al. A systems biology approach towards understanding and treating non-neovascular age-related macular degeneration. *Nat Commun.* 2019;10(1):3347.

8. Fritsche LG, Igl W, Bailey JN, Grassmann F, Sengupta S, Bragg-Gresham JL, et al. A large genome-wide association study of age-related macular degeneration highlights contributions of rare and common variants. *Nat Genet.* 2016;48(2):134-43.

9. van Asten F, Simmons M, Singhal A, Keenan TD, Ratnapriya R, Agron E, et al. A Deep Phenotype Association Study Reveals Specific Phenotype Associations with Genetic Variants in Age-related Macular Degeneration: Age-Related Eye Disease Study 2 (AREDS2) Report No. 14. *Ophthalmology.* 2018;125(4):559-68.

10. van Leeuwen EM, Emri E, Merle BMJ, Colijn JM, Kersten E, Cougnard-Gregoire A, et al. A new perspective on lipid research in age-related macular degeneration. *Prog Retin Eye Res.* 2018;67:56-86.

11. Colijn JM, den Hollander AI, Demirkan A, Cougnard-Gregoire A, Verzijden T, Kersten E, et al. Increased High-Density Lipoprotein Levels Associated with Age-Related Macular Degeneration: Evidence from the EYE-RISK and European Eye Epidemiology Consortia. *Ophthalmology.* 2019;126(3):393-406.

12. Storti F, Klee K, Todorova V, Steiner R, Othman A, van der Velde-Visser S, et al. Impaired ABCA1/ABCG1-mediated lipid efflux in the mouse retinal pigment epithelium (RPE) leads to retinal degeneration. *Elife.* 2019;8.

13. Kaur G, Tan LX, Rathnasamy G, La Cunza NR, Germer CJ, Toops KA, et al. Aberrant early endosome biogenesis mediates complement activation in the retinal pigment epithelium in models of macular degeneration. *Proc Natl Acad Sci U S A.* 2018;115:9014-9.

14. Tan LX, Toops KA, and Lakkaraju A. Protective responses to sublytic complement in the retinal pigment epithelium. *Proc Natl Acad Sci U S A.* 2016;113(31):8789-94.

15. Toops KA, Tan LX, Jiang Z, Radu R, and Lakkaraju A. Cholesterol-mediated activation of acid sphingomyelinase disrupts autophagy in the retinal pigment epithelium. *Mol Biol Cell.* 2015;26:1-14.

16. Yamazaki Y, Zhao N, Caulfield TR, Liu CC, and Bu G. Apolipoprotein E and Alzheimer disease: pathobiology and targeting strategies. *Nature reviews Neurology.* 2019;15(9):501-18.

17. Leduc V, Domenger D, De Beaumont L, Lalonde D, Belanger-Jasmin S, and Poirier J. Function and comorbidities of apolipoprotein e in Alzheimer's disease. *Int J Alzheimers Dis.* 2011;2011:974361.

18. Mahley RW, and Rall SC, Jr. Apolipoprotein E: far more than a lipid transport protein. *Annu Rev Genomics Hum Genet.* 2000;1:507-37.

19. Hatters DM, Peters-Libeu CA, and Weisgraber KH. Apolipoprotein E structure: insights into function. *Trends Biochem Sci.* 2006;31(8):445-54.

20. Toops KA, Tan LX, and Lakkaraju A. Apolipoprotein E Isoforms and AMD. *Adv Exp Med Biol.* 2016;854:3-9.

21. Long JM, and Holtzman DM. Alzheimer Disease: An Update on Pathobiology and Treatment Strategies. *Cell.* 2019;179(2):312-39.

22. Belloy ME, Napolioni V, and Greicius MD. A Quarter Century of APOE and Alzheimer's Disease: Progress to Date and the Path Forward. *Neuron.* 2019;101(5):820-38.

23. Zareparsi S, Reddick AC, Branham KE, Moore KB, Jessup L, Thoms S, et al. Association of apolipoprotein E alleles with susceptibility to age-related macular degeneration in a large cohort from a single center. *Invest Ophthalmol Vis Sci.* 2004;45(5):1306-10.

24. McKay GJ, Patterson CC, Chakravarthy U, Dasari S, Klaver CC, Vingerling JR, et al. Evidence of association of APOE with age-related macular degeneration: a pooled analysis of 15 studies. *Hum Mutat.* 2011;32(12):1407-16.

25. Ishida BY, Bailey KR, Duncan KG, Chalkley RJ, Burlingame AL, Kane JP, et al. Regulated expression of apolipoprotein E by human retinal pigment epithelial cells. *J Lipid Res.* 2004;45 :263-71.

26. Johnson LV, Forest DL, Banna CD, Radeke CM, Maloney MA, Hu J, et al. Cell culture model that mimics drusen formation and triggers complement activation associated with age-related macular degeneration. *Proc Natl Acad Sci U S A.* 2011;108(45):18277-82.

27. Yang P, Skiba NP, Tewkesbury GM, Treboschi VM, Baciu P, and Jaffe GJ. Complement-Mediated Regulation of Apolipoprotein E in Cultured Human RPE Cells. *Invest Ophthalmol Vis Sci.* 2017;58(7):3073-85.

28. Chen X, Singh D, Adelman RA, and Rizzolo LJ. Unstimulated, Serum-free Cultures of Retinal Pigment Epithelium Excrete Large Mounds of Drusen-like Deposits. *Curr Eye Res.* 2020:1-5.

29. Frieden C, Wang H, and Ho CMW. A mechanism for lipid binding to apoE and the role of intrinsically disordered regions coupled to domain-domain interactions. *Proc Natl Acad Sci U S A.* 2017;114(24):6292-7.

30. Alberti S, and Hyman AA. Are aberrant phase transitions a driver of cellular aging? *Bioessays.* 2016;38(10):959-68.

31. Farrer LA, Cupples LA, Haines JL, Hyman B, Kukull WA, Mayeux R, et al. Effects of age, sex, and ethnicity on the association between apolipoprotein E genotype and Alzheimer disease. A meta-analysis. APOE and Alzheimer Disease Meta Analysis Consortium. *JAMA.* 1997;278(16):1349-56.

32. Brzozowska A, Grimholt U, Kulseth MA, Wold I, and Rogne S. The sequence of porcine apolipoprotein E (APOE) cDNA. *DNA Seq.* 1993;4(3):207-10.

33. Lewandowski CT, Maldonado Weng J, and LaDu MJ. Alzheimer's disease pathology in APOE transgenic mouse models: The Who, What, When, Where, Why, and How. *Neurobiol Dis.* 2020;139:104811.

34. Malek G, Johnson LV, Mace BE, Saloupis P, Schmechel DE, Rickman DW, et al. Apolipoprotein E allele-dependent pathogenesis: a model for age-related retinal degeneration. *Proc Natl Acad Sci U S A.* 2005;102(33):11900-5.

35. Levy O, Lavalette S, Hu SJ, Housset M, Raoul W, Eandi C, et al. APOE Isoforms Control Pathogenic Subretinal Inflammation in Age-Related Macular Degeneration. *J Neurosci.* 2015;35(40):13568-76.

36. Lin YT, Seo J, Gao F, Feldman HM, Wen HL, Penney J, et al. APOE4 Causes Widespread Molecular and Cellular Alterations Associated with Alzheimer's Disease Phenotypes in Human iPSC-Derived Brain Cell Types. *Neuron.* 2018;98(6):1294.

37. Zhao J, Davis MD, Martens YA, Shinohara M, Graff-Radford NR, Younkin SG, et al. APOE epsilon4/epsilon4 diminishes neurotrophic function of human iPSC-derived astrocytes. *Hum Mol Genet.* 2017;26(14):2690-700.

38. Rowland HA, Hooper NM, and Kellett KAB. Modelling Sporadic Alzheimer's Disease Using Induced Pluripotent Stem Cells. *Neurochem Res.* 2018;43(12):2179-98.

39. Doss MX, and Sachinidis A. Current Challenges of iPSC-Based Disease Modeling and Therapeutic Implications. *Cells.* 2019;8(5).

40. Toops KA, Tan LX, and Lakkaraju A. A detailed three-step protocol for live imaging of intracellular traffic in polarized primary porcine RPE monolayers. *Exp Eye Res.* 2014;124C:74-85.

41. Li S, Zhang H, Gao P, Chen Z, Wang C, and Li J. A functional mutation at position -155 in porcine APOE promoter affects gene expression. *BMC Genet.* 2011;12:40.

42. Chen Y, Durakoglugil MS, Xian X, and Herz J. ApoE4 reduces glutamate receptor function and synaptic plasticity by selectively impairing ApoE receptor recycling. *Proc Natl Acad Sci U S A.* 2010;107(26):12011-6.

43. Kockx M, Jessup W, and Kritharides L. Regulation of Endogenous Apolipoprotein E Secretion by Macrophages. *Arteriosclerosis, Thrombosis, and Vascular Biology.* 2008;28:1060-7.

44. Coller KE, Heaton NS, Berger KL, Cooper JD, Saunders JL, and Randall G. Molecular determinants and dynamics of hepatitis C virus secretion. *PLoS Pathog.* 2012;8(1):e1002466.

45. Takacs CN, Andreo U, Belote RL, Pulupa J, Scull MA, Gleason CE, et al. Green fluorescent protein-tagged apolipoprotein E: A useful marker for the study of hepatic lipoprotein egress. *Traffic.* 2017;18(3):192-204.

46. Boesze-Battaglia K, and Albert AD. Cholesterol modulation of photoreceptor function in bovine retinal rod outer segments. *J Biol Chem.* 1990;265(34):20727-30.

47. Albert AD, and Boesze-Battaglia K. The role of cholesterol in rod outer segment membranes. *Prog Lipid Res.* 2005;44(2-3):99-124.

48. Fan D, Qiu S, Overton CD, Yancey PG, Swift LL, Jerome WG, et al. Impaired secretion of apolipoprotein E2 from macrophages. *J Biol Chem.* 2007;282(18):13746-53.

49. Huang ZH, Maeda N, and Mazzone T. Expression of the human apoE2 isoform in adipocytes: altered cellular processing and impaired adipocyte lipogenesis. *J Lipid Res.* 2011;52(9):1733-41.

50. Kara E, Marks JD, Fan Z, Klickstein JA, Roe AD, Krogh KA, et al. Isoform- and cell type-specific structure of apolipoprotein E lipoparticles as revealed by a novel Forster resonance energy transfer assay. *J Biol Chem.* 2017;292(36):14720-9.

51. Listenberger LL, and Brown DA. Fluorescent detection of lipid droplets and associated proteins. *Curr Protoc Cell Biol.* 2007;Chapter 24:Unit 24 2.

52. Guziewicz KE, Sinha D, Gomez NM, Zorych K, Dutrow EV, Dhingra A, et al. Bestrophinopathy: An RPE-photoreceptor interface disease. *Prog Retin Eye Res.* 2017;58:70-88.

53. Sabaretnam T, Harris MJ, Kockx M, Witting PK, Le Couteur DG, and Kritharides L. Effects of hydrogen peroxide and apolipoprotein E isoforms on apolipoprotein E trafficking in HepG2 cells. *Clin Exp Pharmacol Physiol.* 2009;36(12):e96-102.

54. Lebrand C, Corti M, Goodson H, Cosson P, Cavalli V, Mayran N, et al. Late endosome motility depends on lipids via the small GTPase Rab7. *EMBO J.* 2002;21(6):1289-300.

55. Mitter SK, Song C, Qi X, Mao H, Rao H, Akin D, et al. Dysregulated autophagy in the RPE is associated with increased susceptibility to oxidative stress and AMD. *Autophagy.* 2014;10(11):1989-2005.

56. Golestaneh N, Chu Y, Xiao YY, Stoleru GL, and Theos AC. Dysfunctional autophagy in RPE, a contributing factor in age-related macular degeneration. *Cell death & disease.* 2017;8(1):e2537.

57. Paun CC, Ersoy L, Schick T, Groenewoud JM, Lechanteur YT, Fauser S, et al. Genetic Variants and Systemic Complement Activation Levels Are Associated With Serum Lipoprotein Levels in Age-Related Macular Degeneration. *Invest Ophthalmol Vis Sci.* 2015;56(13):7766-73.

58. Ferrington DA, Kapphahn RJ, Leary MM, Atilano SR, Terluk MR, Karunadharma P, et al. Increased retinal mtDNA damage in the CFH variant associated with age-related macular degeneration. *Exp Eye Res.* 2016;145:269-77.

59. Wheeler RJ, and Hyman AA. Controlling compartmentalization by non-membrane-bound organelles. *Philos Trans R Soc Lond B Biol Sci.* 2018;373(1747).

60. Bracha D, Walls MT, and Brangwynne CP. Probing and engineering liquid-phase organelles. *Nat Biotechnol.* 2019;37(12):1435-45.

61. Alberti S, and Dormann D. Liquid-Liquid Phase Separation in Disease. *Annu Rev Genet.* 2019;53:171-94.

62. Woodruff JB, Hyman AA, and Boke E. Organization and Function of Non-dynamic Biomolecular Condensates. *Trends Biochem Sci.* 2018;43(2):81-94.

63. Patel A, Lee HO, Jawerth L, Maharana S, Jahnel M, Hein MY, et al. A Liquid-to-Solid Phase Transition of the ALS Protein FUS Accelerated by Disease Mutation. *Cell.* 2015;162(5):1066-77.

64. Molliex A, Temirov J, Lee J, Coughlin M, Kanagaraj AP, Kim HJ, et al. Phase separation by low complexity domains promotes stress granule assembly and drives pathological fibrillization. *Cell.* 2015;163(1):123-33.

65. Gopal PP, Nirschl JJ, Klinman E, and Holzbaur EL. Amyotrophic lateral sclerosis-linked mutations increase the viscosity of liquid-like TDP-43 RNP granules in neurons. *Proc Natl Acad Sci U S A.* 2017;114(12):E2466-E75.

66. Alberti S, Gladfelter A, and Mittag T. Considerations and Challenges in Studying Liquid-Liquid Phase Separation and Biomolecular Condensates. *Cell.* 2019;176(3):419-34.

67. Milovanovic D, Wu Y, Bian X, and De Camilli P. A liquid phase of synapsin and lipid vesicles. *Science.* 2018;361(6402):604-7.

68. Meszaros B, Erdos G, and Dosztanyi Z. IUPred2A: context-dependent prediction of protein disorder as a function of redox state and protein binding. *Nucleic Acids Res.* 2018;46(W1):W329-W37.

69. Elliott DA, Halliday GM, and Garner B. Apolipoprotein-E forms dimers in human frontal cortex and hippocampus. *BMC Neurosci.* 2010;11:23.

70. Yamauchi K, Ebihara Y, and Kawakami Y. Redox status of serum apolipoprotein E and its impact on HDL cholesterol levels. *Clin Biochem.* 2017;50(13-14):777-83.

71. Yamauchi K, and Kawakami Y. The redox status of cysteine thiol residues of apolipoprotein E impacts on its lipid interactions. *Biol Chem.* 2020;401(5):617-27.

72. Rudolf M, Malek G, Messinger JD, Clark ME, Wang L, and Curcio CA. Sub-retinal drusenoid deposits in human retina: organization and composition. *Exp Eye Res.* 2008;87(5):402-8.

73. Mahley RW. Apolipoprotein E: Remarkable Protein Sheds Light on Cardiovascular and Neurological Diseases. *Clin Chem.* 2017;63(1):14-20.

74. Shi Y, and Holtzman DM. Interplay between innate immunity and Alzheimer disease: APOE and TREM2 in the spotlight. *Nat Rev Immunol.* 2018;18(12):759-72.

75. Zhao N, Liu CC, Van Ingelgom AJ, Linares C, Kurti A, Knight JA, et al. APOE epsilon2 is associated with increased tau pathology in primary tauopathy. *Nat Commun.* 2018;9(1):4388.

76. Ostendorf BN, Bilanovic J, Adaku N, Tafreshian KN, Tavora B, Vaughan RD, et al. Common germline variants of the human APOE gene modulate melanoma progression and survival. *Nat Med.* 2020.

77. Pikuleva IA, and Curcio CA. Cholesterol in the retina: The best is yet to come. *Prog Retin Eye Res.* 2014.

78. Sparrow JR. Vitamin A-aldehyde adducts: AMD risk and targeted therapeutics. *Proc Natl Acad Sci U S A.* 2016;113(17):4564-9.

79. Datta S, Cano M, Ebrahimi K, Wang L, and Handa JT. The impact of oxidative stress and inflammation on RPE degeneration in non-neovascular AMD. *Prog Retin Eye Res.* 2017;60:201-18.

80. Crabb JW, Miyagi M, Gu X, Shadrach K, West KA, Sakaguchi H, et al. Drusen proteome analysis: An approach to the etiology of age-related macular degeneration. *Proc Natl Acad Sci U S A.* 2002;99(23):14682-7.

81. Pilgrim MG, Lengyel I, Lanzirotti A, Newville M, Fearn S, Emri E, et al. Subretinal Pigment Epithelial Deposition of Drusen Components Including Hydroxyapatite in a Primary Cell Culture Model. *Invest Ophthalmol Vis Sci.* 2017;58(2):708-19.

82. Bergen AA, Arya S, Koster C, Pilgrim MG, Wiatrek-Moumoulidis D, van der Spek PJ, et al. On the origin of proteins in human drusen: The meet, greet and stick hypothesis. *Prog Retin Eye Res.* 2018.

83. Werb Z, Takemura R, Stenberg PE, and Bainton DF. Directed exocytosis of secretory granules containing apolipoprotein E to the adherent surface and basal vacuoles of macrophages spreading on immobile immune complexes. *Am J Pathol.* 1989;134(3):661-70.

84. Shiki A, Inoh Y, Yokawa S, and Furuno T. Promotion of microtubule acetylation plays an important role in degranulation of antigen-activated mast cells. *Inflamm Res.* 2019;68(3):181-4.

85. Rawat V, Wang S, Sima J, Bar R, Liraz O, Gundimeda U, et al. ApoE4 Alters ABCA1 Membrane Trafficking in Astrocytes. *J Neurosci.* 2019;39(48):9611-22.

86. Gehlbach P, Li T, and Hatef E. Statins for age-related macular degeneration. *Cochrane Database Syst Rev.* 2016(8):CD006927.

87. Vavvas DG, Daniels AB, Kapsala ZG, Goldfarb JW, Ganotakis E, Loewenstein JI, et al. Regression of Some High-risk Features of Age-related Macular Degeneration (AMD) in Patients Receiving Intensive Statin Treatment. *EBioMedicine.* 2016;5:198-203.

88. Donnelly LA, Palmer CN, Whitley AL, Lang CC, Doney AS, Morris AD, et al. Apolipoprotein E genotypes are associated with lipid-lowering responses to statin treatment in diabetes: a Go-DARTS study. *Pharmacogenet Genomics.* 2008;18(4):279-87.

89. van Leeuwen R, Tomany SC, Wang JJ, Klein R, Mitchell P, Hofman A, et al. Is medication use associated with the incidence of early age-related maculopathy? Pooled findings from 3 continents. *Ophthalmology.* 2004;111(6):1169-75.

90. Yin C, Ackermann S, Ma Z, Mohanta SK, Zhang C, Li Y, et al. ApoE attenuates unresolvable inflammation by complex formation with activated C1q. *Nat Med.* 2019;25(3):496-506.

91. Nissila E, Hakala P, Leskinen K, Roig A, Syed S, Van Kessel KPM, et al. Complement Factor H and Apolipoprotein E Participate in Regulation of Inflammation in THP-1 Macrophages. *Front Immunol.* 2018;9:2701.

92. Chung WS, Verghese PB, Chakraborty C, Joung J, Hyman BT, Ulrich JD, et al. Novel allele-dependent role for APOE in controlling the rate of synapse pruning by astrocytes. *Proc Natl Acad Sci U S A.* 2016;113(36):10186-91.

93. Wu L, Zhang X, and Zhao L. Human ApoE Isoforms Differentially Modulate Brain Glucose and Ketone Body Metabolism: Implications for Alzheimer's Disease Risk Reduction and Early Intervention. *J Neurosci.* 2018;38(30):6665-81.

94. Liu L, MacKenzie KR, Putluri N, Maletic-Savatic M, and Bellen HJ. The Glia-Neuron Lactate Shuttle and Elevated ROS Promote Lipid Synthesis in Neurons and Lipid Droplet Accumulation in Glia via APOE/D. *Cell Metab.* 2017;26(5):719-37 e6.

95. Ioannou MS, Jackson J, Sheu SH, Chang CL, Weigel AV, Liu H, et al. Neuron-Astrocyte Metabolic Coupling Protects against Activity-Induced Fatty Acid Toxicity. *Cell.* 2019;177(6):1522-35 e14.

96. van Niel G, Bergam P, Di Cicco A, Hurbain I, Lo Cicero A, Dingli F, et al. Apolipoprotein E Regulates Amyloid Formation within Endosomes of Pigment Cells. *Cell reports.* 2015;13(1):43-51.

97. Keenan TD, Agron E, Domalpally A, Clemons TE, van Asten F, Wong WT, et al. Progression of Geographic Atrophy in Age-related Macular Degeneration: AREDS2 Report Number 16. *Ophthalmology.* 2018;125(12):1913-28.

98. Sparrow JR, Parish CA, Hashimoto M, and Nakanishi K. A2E, a lipofuscin fluorophore, in human retinal pigmented epithelial cells in culture. *Invest Ophthalmol Vis Sci.* 1999;40:2988-95.

99. Lakkaraju A, Finnemann SC, and Rodriguez-Boulan E. The lipofuscin fluorophore A2E perturbs cholesterol metabolism in retinal pigment epithelial cells. *Proc Natl Acad Sci U S A.* 2007;104(26):11026-31.

100. Abbas RO, and Azzazy HM. Association of single nucleotide polymorphisms in CFH, ARMS2 and HTRA1 genes with risk of age-related macular degeneration in Egyptian patients. *Ophthalmic Genet.* 2013;34(4):209-16.

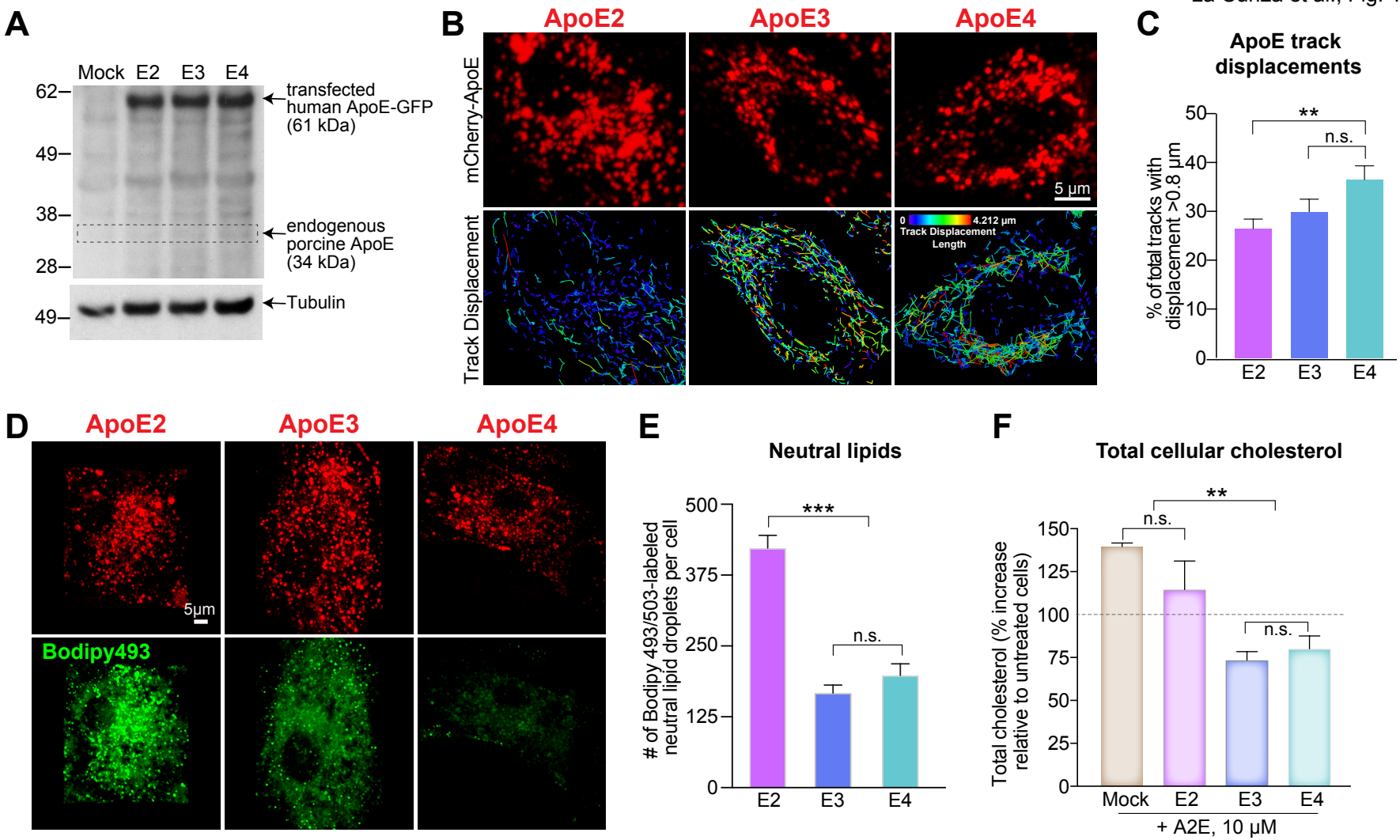

Figure 1. Isoform-specific ApoE trafficking and cholesterol transport in the RPE. (A) Representative immunoblot of ApoE in porcine primary RPE transfected with EGFP-tagged human ApoE2, E3, or E4. Arrows: 61 kDa fusion proteins, 34 kDa endogenous ApoE and tubulin as loading control. **(B)** Stills from live imaging of mCherry-tagged human ApoE2, E3, or E4 (top panel, red) in primary RPE cultures. Scale bar = 5 µm. Lower panel: tracks of individual ApoE vesicles. Color bar shows displacement length of individual tracks from short (cooler colors) to long (warmer colors), range 0.0 µm to 4.212 µm. **(C)** Percent of total ApoE tracks with displacement greater than 0.8 µm in ApoE2, E3 or E4-expressing RPE. Mean ± SEM, n > 17 cells per condition from three independent experiments. **, $p < 0.02$. **(D)** Representative images from live imaging and **(E)** quantification of Bodipy 493/503-labeled neutral lipids in ApoE2, E3 or E4-expressing RPE. Mean ± SEM, n > 47 cells per condition, ***, $p < 0.0001$. **(F)** Quantification of endogenous cholesterol content in mock-transfected or ApoE2, E3 or E4-expressing RPE treated with A2E. Mean ± SEM, pooled data from three independent experiments, **, $p < 0.001$. C, E and F: one-way ANOVA with Bonferroni post-test. n.s. – not significant. See also Figure S1.

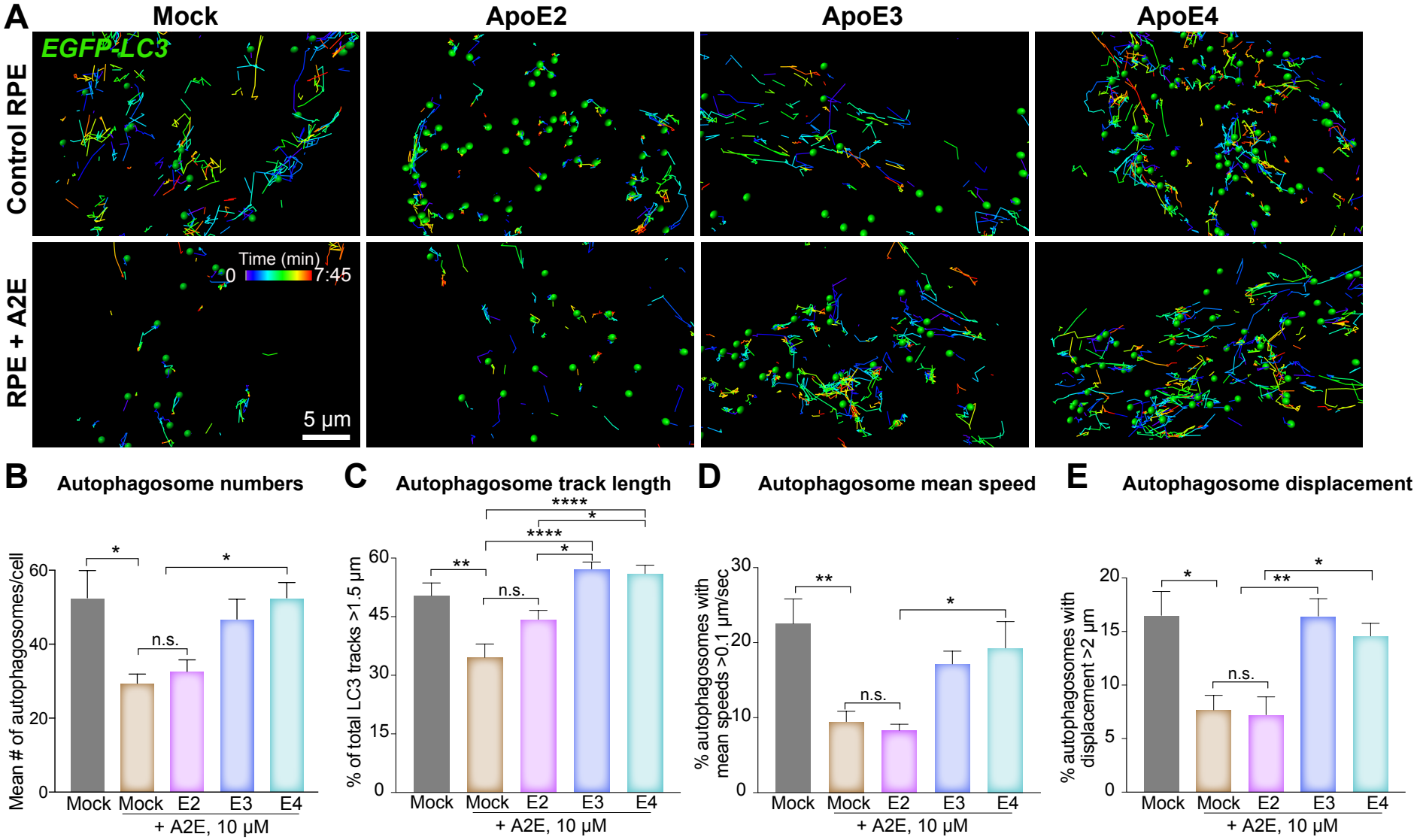

Figure 2. ApoE2 aggravates autophagic defects induced by lipofuscin bisretinoids. (A) Stills from spots and tracks analyses of live imaging of EGFP-LC3 autophagosome trafficking in mock-transfected or ApoE2, E3 or E4-expressing RPE, treated or not with A2E. **(B)** Average number of EGFP-LC3 autophagosomes per cell. **(C)** Percent of total EGFP-LC3 tracks longer than 1.5 µm. **(D)** Percent of autophagosomes with mean speeds > 0.1 µm/sec. **(E)** Percent of autophagosomes with displacement > 2 µm in mock-transfected or ApoE2, E3 or E4-expressing RPE, treated or not with A2E. Mean ± SEM, n >13 cells per condition. *, $p < 0.05$, **, $p < 0.005$, ***, $p < 0.001$ and ****, $p < 0.0001$. n.s. not significant. One-way ANOVA with Bonferroni post-test. See also Figure S2 and Movies S1-S8.

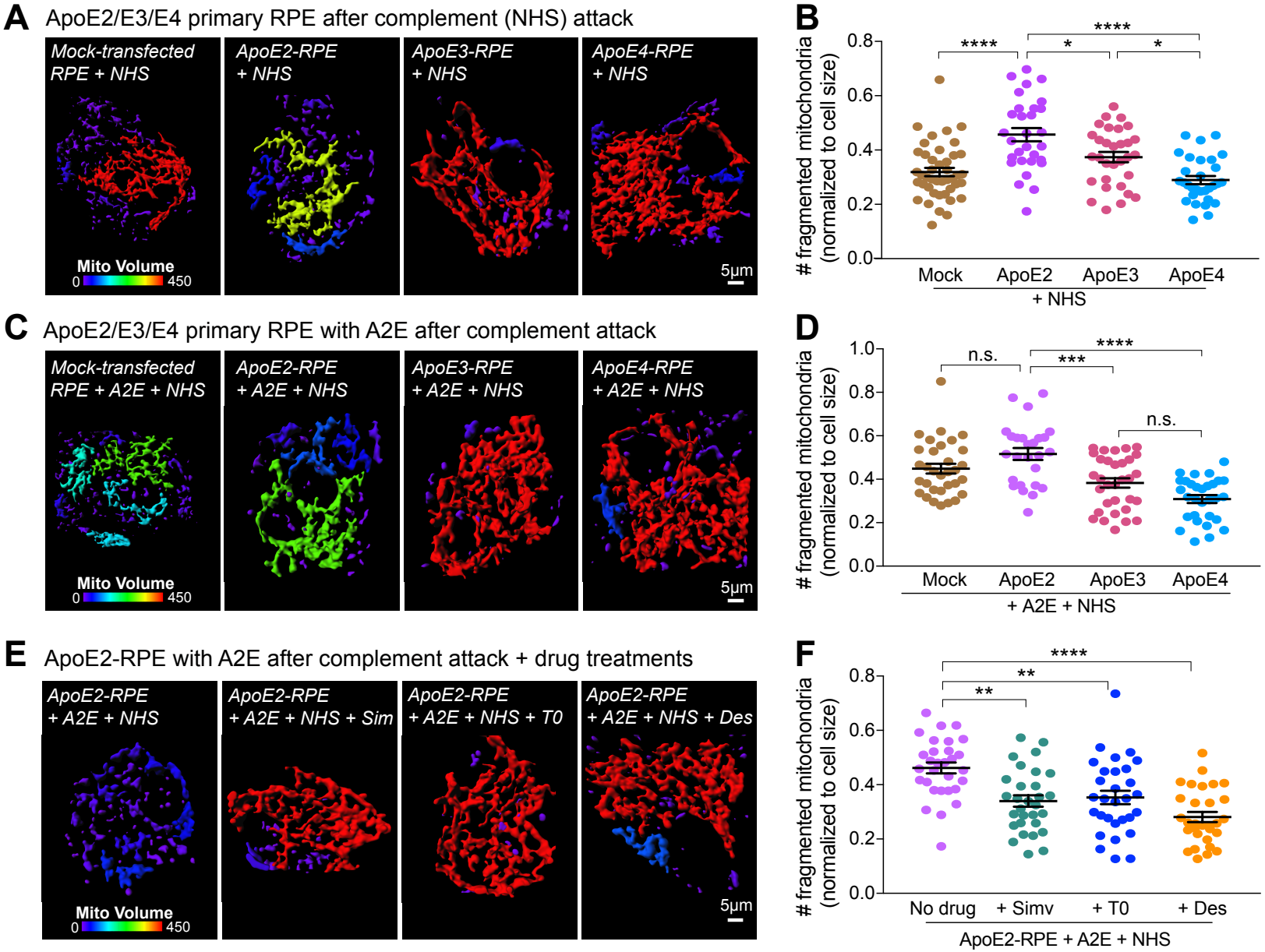

Figure 3. ApoE2 exacerbates complement-induced mitochondrial fragmentation in the RPE. (A) 3D reconstruction of mitochondrial volumes from live imaging of Mitotracker-labeled mitochondria in mock-transfected or ApoE2, E3 or E4-expressing RPE exposed to 10% NHS to induce complement attack. Color bar: cooler colors indicate increasing mitochondrial fragmentation. **(B)** Number of fragmented mitochondria per cell after NHS exposure. **(C)** Mitochondrial volumes as in (A) in RPE treated with A2E prior to NHS exposure. **(D)** Quantification of mitochondrial fragments as in (B). **(E)** Mitochondrial volumes as in (A) in ApoE2-expressing RPE with A2E exposed to NHS and treated with Simvastatin (5 µM, 16 h), T0901317 (1 µM, 16 h) or desipramine (10 µM, 3 h) prior to imaging. **(F)** Quantification of mitochondrial fragments as in (B). Mean ± SEM, *, $p < 0.05$; **, $p < 0.005$; ***, $p < 0.0005$; ****, $p < 0.0001$. n = 30 cells (A), 26 cells (B) and 30 cells (C) per condition; One-way ANOVA with Bonferroni post-test; See also Figure S3.

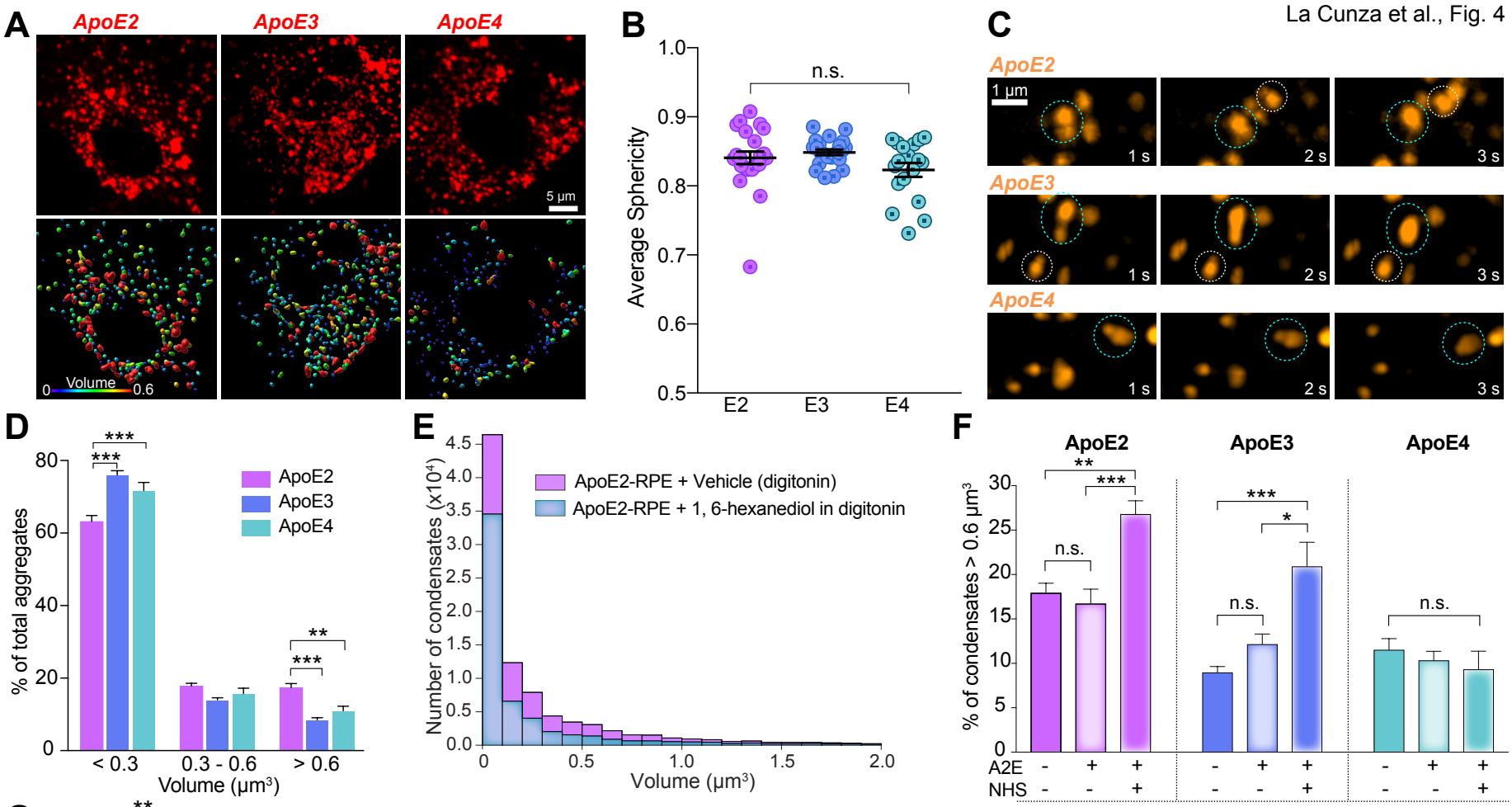

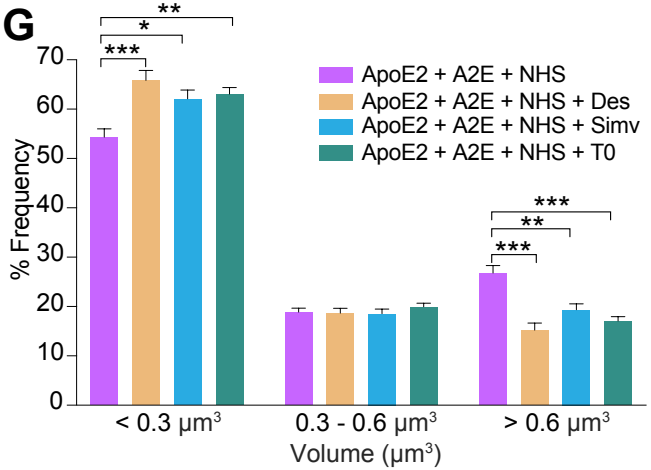

Figure 4. ApoE2 undergoes phase separation due to mitochondrial stress in the RPE. **(A)** Representative stills (top panel) and 3D volume reconstructions (lower panel) from live imaging of intracellular ApoE2, E3 or E4 in the RPE. Warmer colors indicate larger volumes. **(B)** Average sphericity of ApoE condensates in RPE expressing ApoE2, E3 or E4. Mean ± SEM, n=17-23 cells per condition. n.s. - not significant. **(C)** Time-lapse imaging shows that ApoE condensates exhibit liquid behavior by fusing with each other (dotted circles). **(D)** Frequency distribution of condensate volumes in ApoE2, E3 or E4 expressing RPE. **(E)** Number and volume of condensates in ApoE2-expressing RPE treated with 1,6-hexanediol,which disrupts weak hydrophobic interactions (blue bars) or with vehicle (digitonin, magenta bars) alone. **(F)** Frequency distribution of condensates with volumes greater than 0.6 µm³ in RPE expressing ApoE2, E3 or E4 and treated or not with NHS and A2E. **(G)** Frequency distribution of condensate volumes in ApoE2-expressing RPE with A2E and NHS, and treated with Simvastatin (5 µM, 16 h), T0901317 (1 µM, 16 h) or desipramine (10 µM, 3 h). Mean ± SEM, *, $p < 0.05$; **, $p < 0.005$; ***, $p < 0.0001$. n = 15-29 cells per condition; One-way ANOVA with Bonferroni post-test. See also Figure S4.

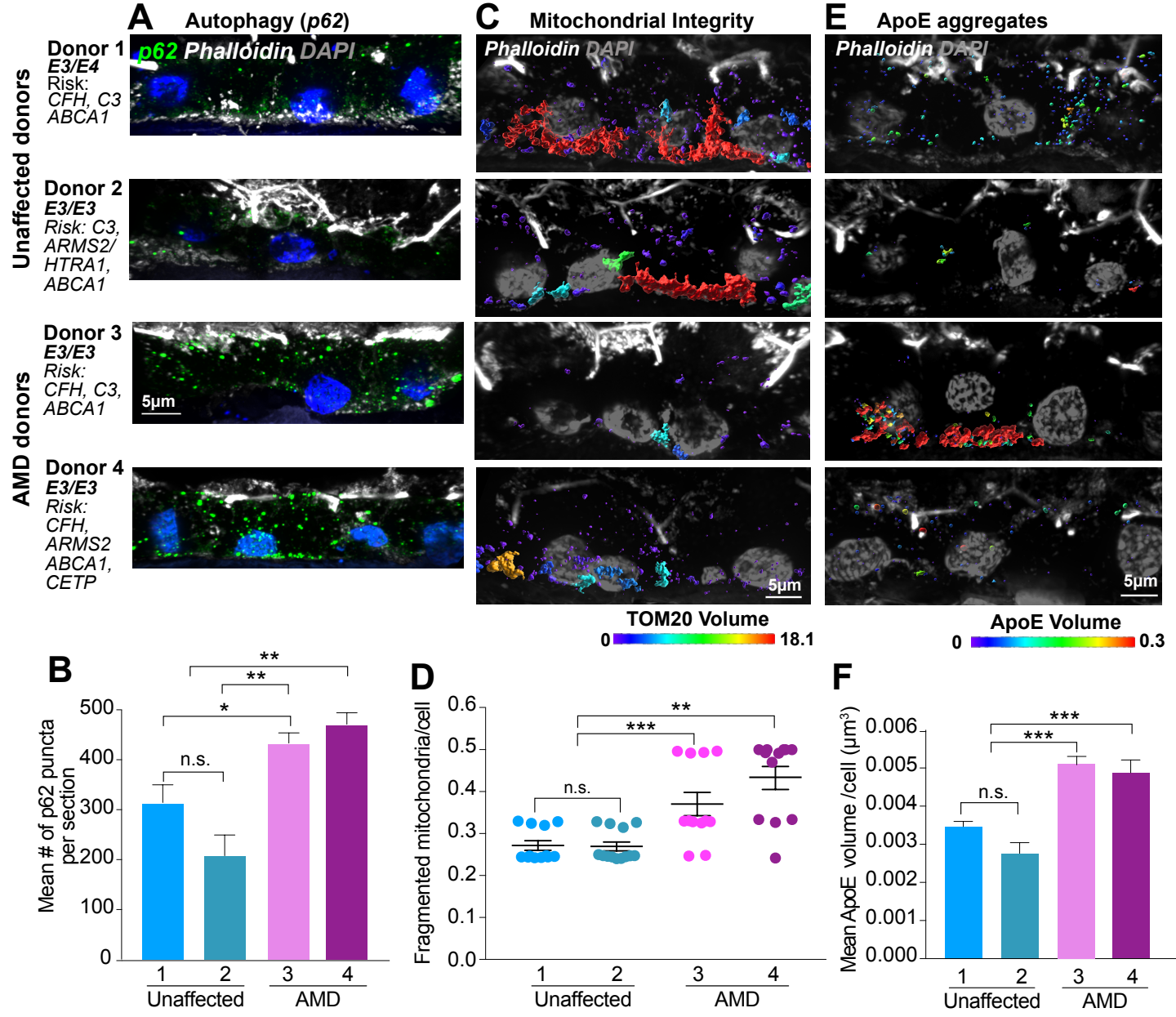

Figure 5. Impaired autophagy, fragmented mitochondria, and intracellular ApoE aggregates in RPE from human donors with AMD. (A) Representative images of p62 immunostaining (green) and **(B)** quantification of p62 puncta in cryosections of the macula from unaffected donors and donors with AMD. Only the RPE monolayer is shown. Phalloidin (white) and DAPI (blue (5A) and grey (5C & E)). Mean ± SEM, *, $p < 0.05$; **, $p < 0.01$. Multiple *t*-test with Welch's correction for unequal variances. **(C)** Representative surface reconstructions of TOM20-stained mitochondrial networks in RPE from unaffected and AMD donors. **(D)** Quantification of fragmented mitochondria per cell from images in A. Mean ± SEM, **, $p < 0.005$; ***, $p < 0.0001$. One-way ANOVA with Bonferroni post-test; **(E)** Representative surface reconstructions of ApoE-labeled aggregates in RPE from unaffected donors and donors with AMD. **(F)** Quantification of ApoE aggregate volumes per cell from images in C. Mean ± SEM, ***, $p < 0.0001$. Multiple *t*-test with Welch's correction. See also Figure S5 and Tables S2 and S3.

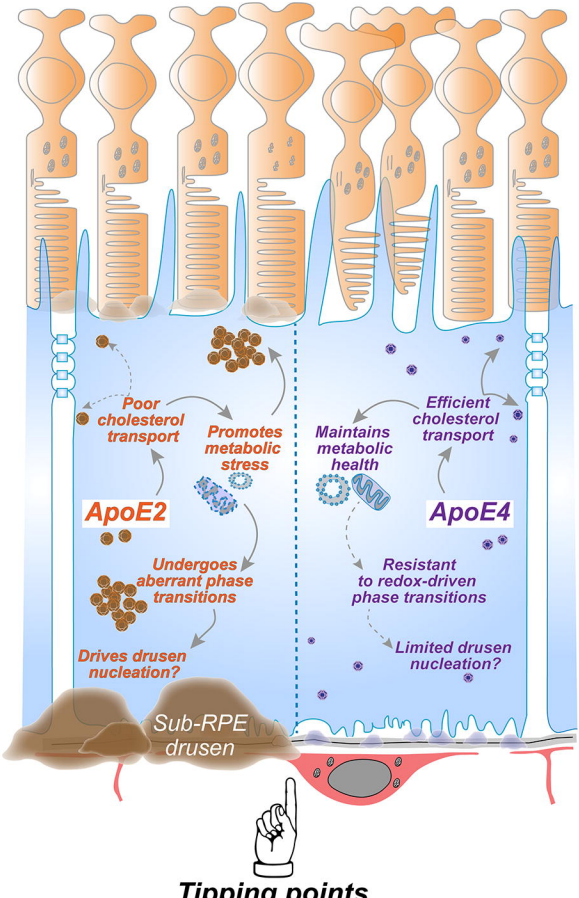

Tipping points

APOE allelic variants regulate RPE homeostasis